Chapter 5

Pb doped TiO_2 ($Pb_xTi_{1-x}O_2$) thin films for a solid-state solar cell application

5.1 Introduction

After Gratzel's low-cost high-efficiency photoelectrochemical (PEC) solar cell, based on dye-sensitized nanocrystalline TiO_2 thin film [1], much attention has been drawn to this classical material for its use in solar to electrical energy conversion. Although efficiencies of around 10% have been reported for Gratzel PEC cell, it suffers a lack of stability due to liquid electrolyte and, until now, commercialization of the cell has not been realized.

Considering the high efficiency of dye-sensitized TiO_2 PEC cell at one hand and the low stability on the other, one may well look into the prospect of developing a low-cost solid-state solar cell using this material. In the previous chapter, we have proposed a theoretical model for a solid-state solar cell based on TiO_2 ($Pb_xTi_{1-x}O_2$) where $CuInSe_2$ has been used as the absorber material. Lead (Pb) has been used as a dopant in TiO_2 in order to reduce the high barrier height ($\Delta E_C = 0.48$ eV) at $TiO_2/CuInSe_2$ heterojunction, due to the large mismatch between the conduction band positions of the two materials, which hinders the flow of photogenerated electrons from $CuInSe_2$ to TiO_2 and limits the theoretical efficiency of $n-TiO_2/p-CuInSe_2$ cell to a very low value (1.51%). By incorporating Pb into TiO_2 lattice, both the band gap and electron affinity of TiO_2 can be varied and consequently the spike ΔE_C can be reduced [2, 3]. Our theoretical calculation reveals that efficiency as high as 18% can be obtained for $n-Pb_xTi_{1-x}O_2/p-CuInSe_2$ solar cell, provided electron affinities of the two materials

match perfectly and there are no resistivity losses.

Krishna *et al.* showed in their theoretical work the possibility of gradual reduction in the band gap and increase in the electron affinity of TiO_2 with the addition of increased amount of Pb [3]. Furthermore, they studied the bulk properties of Pb doped TiO_2 prepared by solid state sintering of PbO_2/TiO_2 mixture and reported the formation of mixed phases due to high sintering temperatures [4,5]. As an alternative, we have adopted sol–gel method, known to be a low temperature technique, in order to obtain a single phase Pb doped TiO_2 and also in the form of thin film which will be useful for the application of optoelectronic devices such as solar cells. In this direction, we have prepared both pure and Pb doped TiO_2 thin films by a simple sol–gel method and preliminary investigation of these films shows a gradual decrease in the band gap as TiO_2 is doped with increased amount of Pb[6]. Howeover, presence of both anatase and rutile phases is observed for all the films and crystallinity degrades as the amount of Pb into TiO_2 increases.

In this chapter, we will report the results on our continued efforts towards the preparation of single phase Pb doped TiO_2 thin films of anatase type which is reported to have superior opto-electrical properties than those of rutile [7,8]. Lead acetate trihydrate, $Pb(CH_3COO)_2.3H_2O$, and titanium tri-isopropoxide mono-acetylacetonate, $Ti(C_3H_7O)_3(CH_3COCHCOCH_3)$, hereafter called TIAA, which had been reported to give good stability and better control of viscosity by different authors [9–11], are used as the source materials for Pb and Ti, respectively, instead of lead nitrate, $Pb(NO_3)_2$, and titanium tetra-isopropoxide, $Ti(C_3H_7O)_4$, which were used earlier [6]. Using this modified sol-gel method, 5 and 10 mol % Pb doped TiO_2 thin films are prepared. Optical properties of the films are studied by transmission spectroscopy and photoluminescence (PL) spectroscopy. A detailed structural, compositional and valence state analyses by X –ray diffraction (XRD), scanning electron microscopy (SEM) attached with an energy dispersive X-ray analysis (EDAX) and X –ray photoelectron spectroscopy (XPS) have also been carried out for the 10 mol % Pb doped TiO_2 thin film which shows larger decrease in the band gap. Details of the experimental techniques and the analyses of various results are discussed in the following sections.

5.2 Experimental

5.2.1 *Film preparation*

Pure and Pb doped (5 and 10 mole %) TiO_2 thin films have been prepared by a simple sol –gel dip –coating method. Figure 5.1 illustrates the schematic flow diagram for the preparation of the sol solution and the thin films of Pb doped TiO_2. Details of the sol solution preparation for the pure TiO_2 is same as discussed in section 2.2 of chapter 2.

Lead acetate trihydrate (0.025 mol) and 2-methoxyethanol (50 ml) were mixed in a three-neck flux and distilled at 130 °C until 20 ml of liquid was trapped in the distillation trap. Distillation was performed at 126 °C for a couple of hours with flowing nitrogen gas during which hydrous lead acetate dissolves in methoxyethanol. The dehydrated solution (30 ml) was cooled to 60 °C and then 0.225 mol of TIAA, prepared by equimolar reaction of titanium tetra-isopropoxide and acetylacetone, was added dropwise through a funnel, with constant stirring. The resulting solution was refluxed and distilled at 110 °C for 4 hours to promote complexation and eliminate alkylacetate, a by-product of the reaction. The resulting solution was cooled to room temperature and methoxyethanol was added to make the total volume of the solution 100 ml. The solution, which was brown in color, was stored in abottle filled with dried nitrogen gas and kept in a desiccator.

A precursor sol solution of Pb –Ti –O system, with molar concentration of 0.5 mol/l, was prepared by diluting 10 ml of Pb –TIAA solution with 25 ml of methoxyethanol and carrying out hydrolysis and polycondensation reactions by adding H_2O and HNO_3 diluted in methoxyethanol (15 ml), and heating the solution for 24 h. The amount of water and nitric acid added was defined as the number of moles added to one mole of titanium dissolved in the alkoxide solution: $[H_2O]/Ti$ and $[NO_3]/Ti$, respectively. These molar ratios of water and nitric acid added were 4 and 0.1, respectively. All the reactions were carried out in N_2 atmosphere.

Films were coated on single crystal Si (100) and fused quartz substrates by dip – coating method with a pulling speed of 0.1 mm/sec and heat-treated at 250 °C for 15 minutes. This process

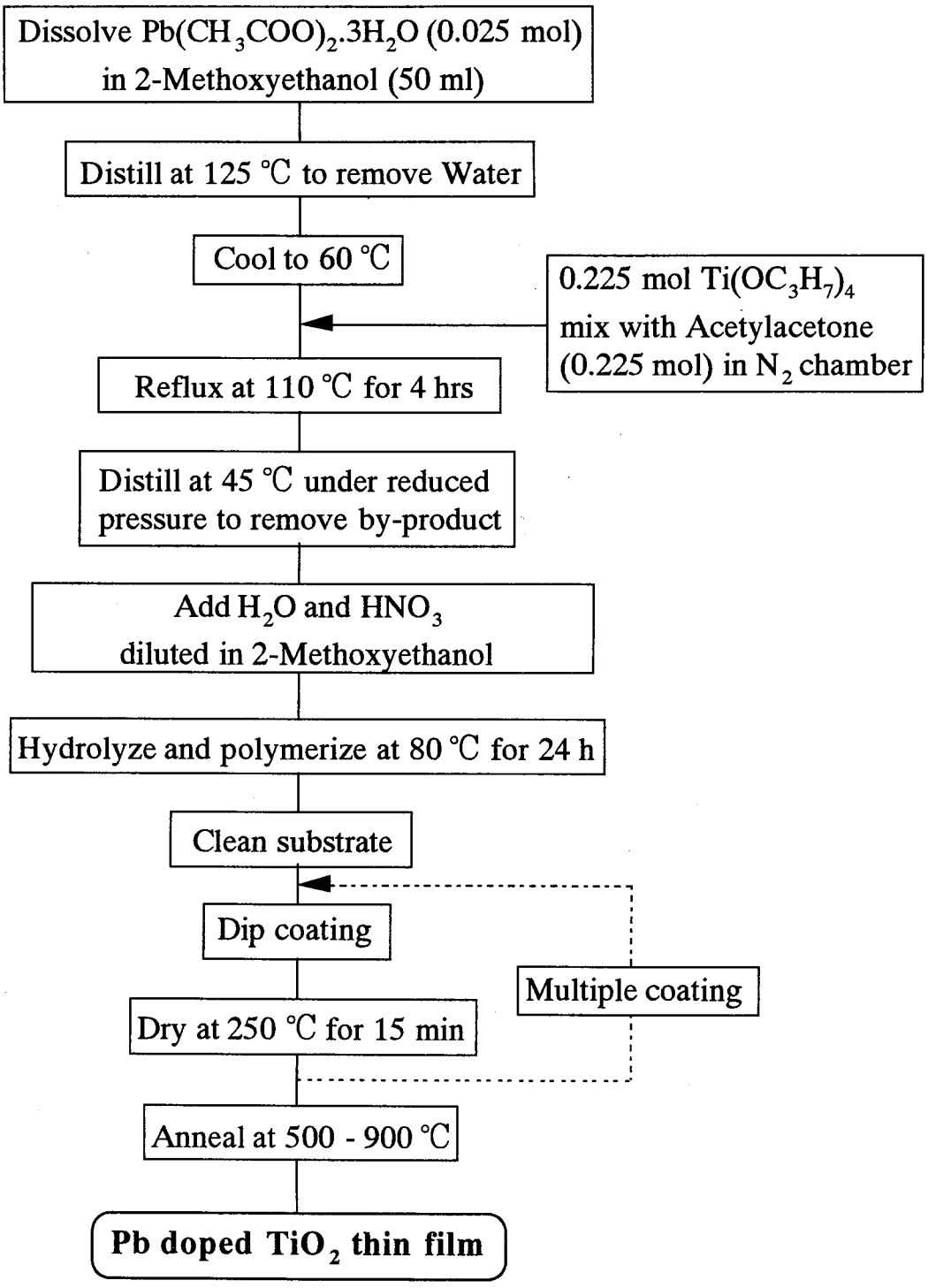

Fig. 5.1. Flow diagram for the preparation of Pb doped TiO_2 thin films by sol–gel method.

was repeated 10 times and finally the multi-coated films were annealed at different (500 °C to 900 °C) temperatures at a constant heating rate of 5 °C min^{-1} for phase formation and crystallization. While the films deposited on Si substrate were crystalline anatase type when annealed at 500 °C, they were

amorphous when deposited on fused quartz substrate at the same temperature. For films deposited on fused quartz, crystallization took place at around 600 °C and for both Si and fused quartz substrates, films were anatse type up to 600 °C above which formation of rutile phase was also observed along with the anatase phase. Therefore, in this report we have restricted our discussion on 600 °C annealed films which contains only anatase modification of TiO_2.

5.2.2 *Characterization*

Transmission spectrum of the samples in the wavelength range of 340 to 800 nm was recorded using a UV/VIS/NIR spectrophotometer (JASCO V – 570). Photoluminescence was measured at liquid nitrogen temperature using 325 nm He–Cd laser source. Crystallinity and phase analyses of the films were carried out by X-ray diffraction (Rint 2000) with an accelerating potential of 40 kV and current of 35 mA using CuKα radiation (1.54056 Å) as an X-ray source. All the patterns were recorded at a scanning rate of $0.5°\,min^{-1}$ by steps of $0.02°$ in the standard $\theta-2\theta$ geometry. The surface morphology, cross-sectional view and the compositional distribution of the films were observed by a high resolution scanning electron microscope (Hitachi S-5000) attached with an energy dispersive X–ray analysis. Depth profiling, composition and valence state analyses of various species present in the film were carried out by an X–ray photoelectron spectroscope with an $AlK\alpha_{1,2}$ radiation, where an Ar^+ ion beam with an accelerating potential of 3 keV and a beam current of 3 mA was used to etch the film.

5.3 Results and discussion

5.3.1. *Transmission spectroscopy*

The transmission spectra of pure, and 5 and 10 mol % Pb doped TiO_2 thin films deposited on fused quartz substrate, together with that of the bare substrate, are shown in Fig. 5.2. The transmission of the bare fused quartz is greater than 92% over the entire spectral region. The transmission spectra of the samples with TiO_2 and Pb doped TiO_2 films on fused quartz show quite a

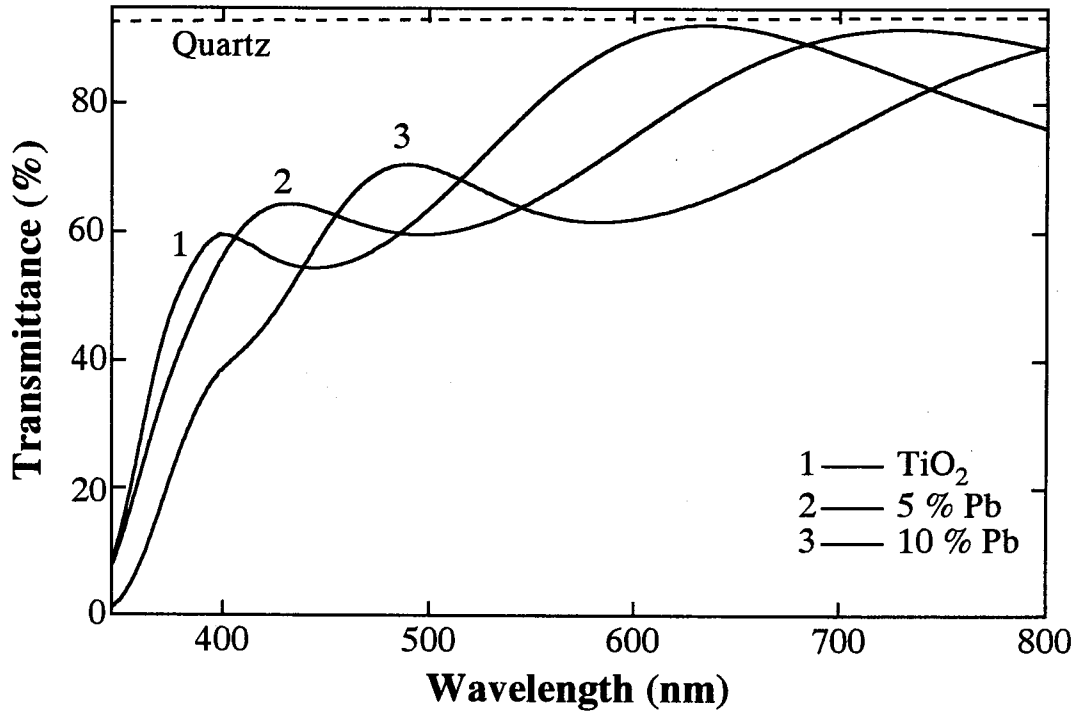

Fig. 5.2 Transmission spectra of pure and 5 and 10 mol % Pb doped TiO_2 thin films deposited on quartz substrate and annealed at 600 °C, showing gradual shift of the spectra towards longer wavelength region as TiO_2 is doped with increased amount of Pb.

different feature. For pure TiO_2 transmittance is as low as 76% at longer wavelengths (800 nm) and gradually rises at shorter wavelengths until it reaches its maximum value of 92.41% at 633 nm, a value very close to that of the bare fused quartz subatrate (92.46%). At shorter wavelengths, the transmittance decreases rather quickly, shows a shoulder near 395 nm and approaches near zero at around 350 nm. The wave nature of the transmittance between 800 and 395 nm is due to the interference between the TiO_2 film and the substrate. On the other hand, the fast decrease below 395 nm is due to absorption of light caused by the excitation of electrons from the valence band to the conduction band of TiO_2. The absorption edge shifts towards longer wavelengths for 5 and 10 mol% Pb doped TiO_2 and clearly indicates gradual decrease in the optical gap of TiO_2 as it is doped with increased amount of Pb. To have an estimate of the optical gap energies, absorption coefficient (α) of the films, near the absorption edge, were calculated from the transmittance (T) and reflectance (R) data using the simplified relation $T=(1-R)^2e^{-\alpha d}/(1-R^2e^{-2\alpha d})$, where d is the thickness of the films [7].

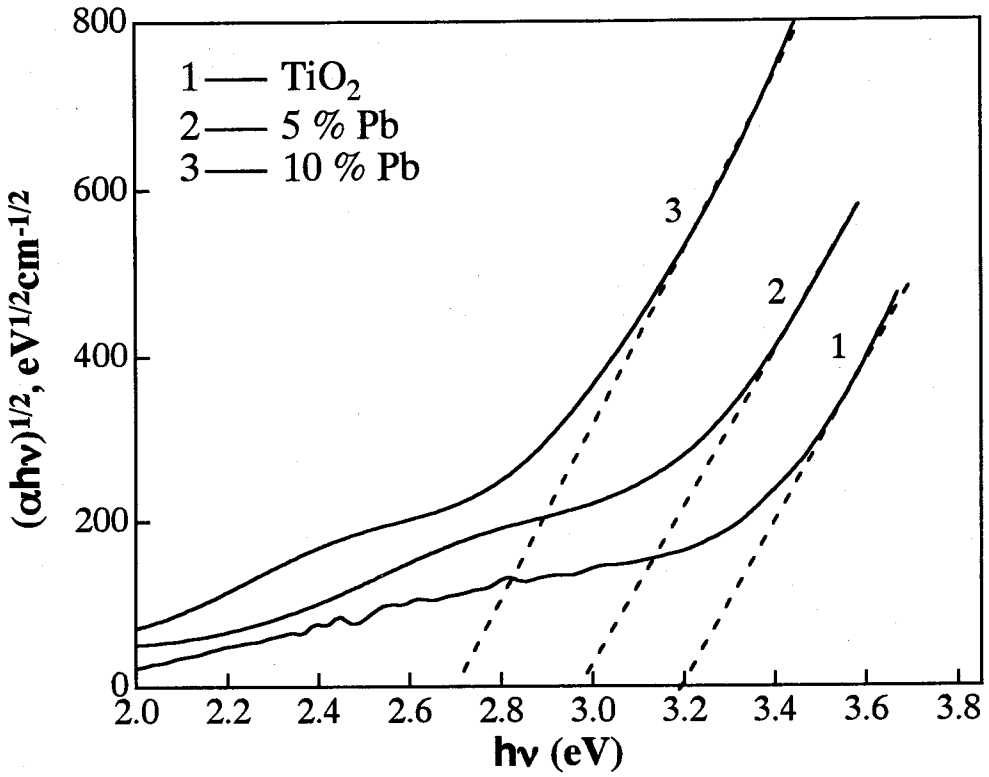

Fig. 5.3 Plots of $(\alpha h\nu)^{1/2}$ *vs.* $h\nu$ for pure, and 5 and 10 mol % Pb doped TiO_2 thin films deposited on vitreous silica substrate.

The intercept of the tangent to the $(\alpha h\nu)^{1/2}$ *vs.* $h\nu$ plot, where $h\nu$ is the photon energy, will give an estimate of the optical gap energies for polycrystalline materials such as TiO_2. Plots of $(\alpha h\nu)^{1/2}$ *vs.* $h\nu$ are drawn for all the films and are shown in Fig. 5.3. The gap energies estimated from the intercept of the tangents to the plots are 3.2, 2.95, and 2.7 eV for pure, and 5 and 10 mol% Pb doped TiO_2, respectively. While the optical gap of pure TiO_2 is in very good agreement with those reported in the literature for anatase TiO_2, gaps obtained for Pb incorporated TiO_2 show a clear decrease from that of pure TiO_2 which are 0.25 and 0.5 eV for 5 and 10 mol % Pb doped TiO_2, respectively.

5.3.2 *Photoluminescence spectroscopy*

An intense yellowish green luminescence spectrum with broad spectral width has been observed for pure TiO_2 as shown in Fig. 5.4. This spectrum resembles the luminescence spectrum of both single and polycrystalline TiO_2 reported by others [7,8]. The large difference between the band gap energy (~3.14 eV) and the emission peak energy (2.48 eV), which is around 0.66 eV, is described as the Stokes shift due to the Frank-Condon effect.

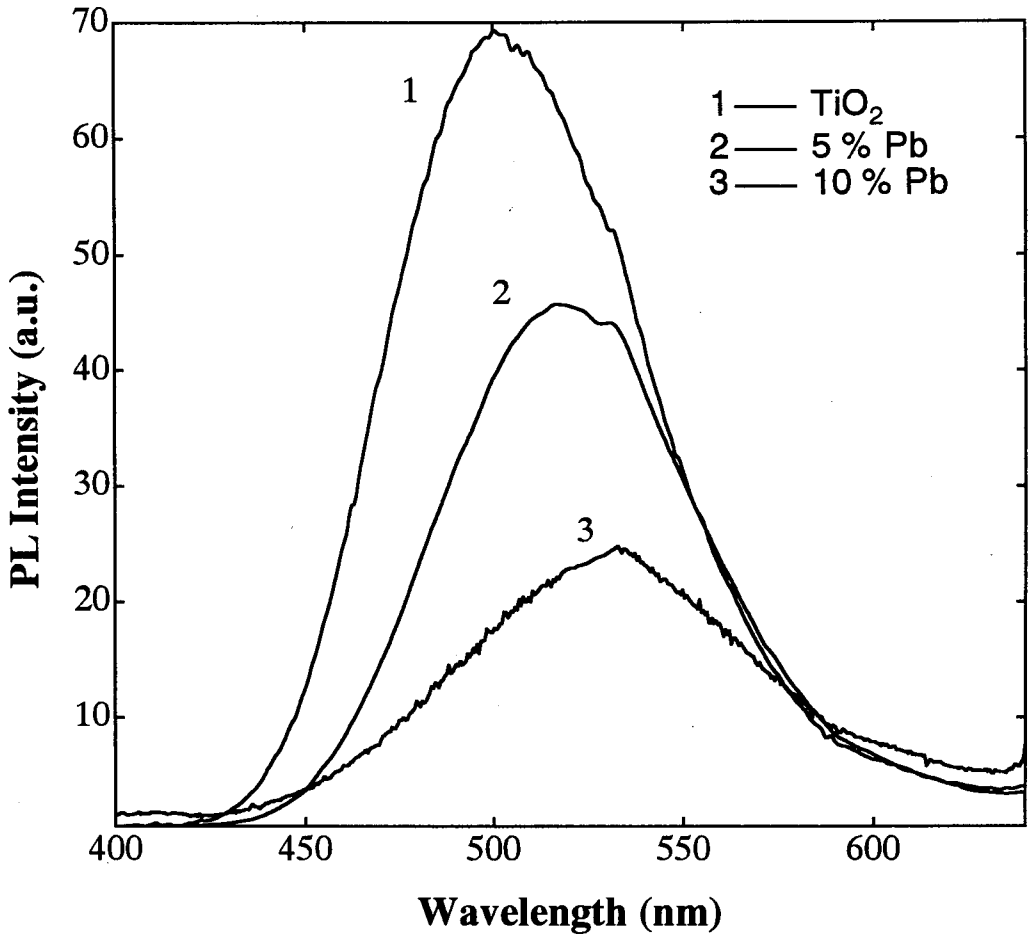

Fig. 5.4 Photoluminescence spectrum of pure, and 5 and 10 mol % Pb doped TiO_2 thin films, deposited on Si substrate, measured at 77 K.

There is a gradual shift of the emission peak towards longer wavelength region and decrease in the peak intensity with increased amount of Pb incorporation into TiO_2 (see Fig. 5.4). The shift of the emission peak towards longer wavelengths, i.e., lower energy region, further supports the lowering of the band gap of TiO_2 with Pb doping. Decrease in emission intensity with Pb doping may be due to the introduction of new defect sites that enhances non-radiative recombination of the excited electrons. Similar quenching in the luminescence intensity has also been observed for In and Ce doped TiO_2 by Tang *et al.* [8].

5.3.3 *X−ray diffraction*

The X−ray diffraction (XRD) patterns of pure and 10 mol % Pb doped TiO_2 thin films,

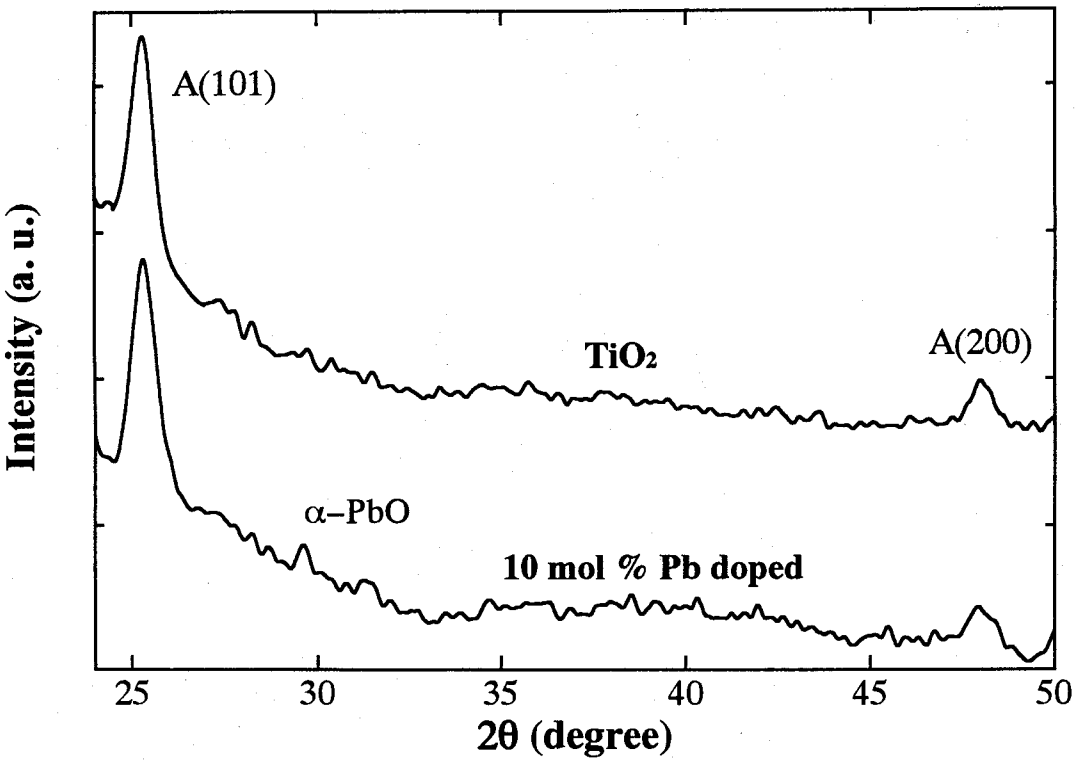

Fig. 5.5 X–ray diffraction patterns of (a) pure and (b) 10 mol % Pb doped TiO_2 thin films deposited on Si substrate. (A : anatase).

deposited on Si substrate, are shown in Fig. 5.5. The films show polycrystalline nature with crystals oriented mostly in (101) plane of anatase (A) phase of TiO_2 lattice. A slight shift in the d spacing observed for the Pb doped film confirms the incorporation of Pb into TiO_2. The initial hump, present in both the patterns, is due to the slide glass which was used to hold the samples. The d values of A(101) and A(200) planes for both pure and 10 mol % Pb doped TiO_2 and the corresponding lattice parameters, a and c, are summerized in Table 5.1. The lattice parameters obtained for pure TiO_2 are in good agreement with those given in the literature [12]. In addition to the X–ray peaks corresponding to A(101) and A(200) reflections, a small X–ray peak corresponding to (101) reflection of α–PbO

Table 5.1 d values and the lattice constants, a and c, of pure and 10 mol % Pb doped TiO_2 ($Pb_xTi_{1-x}O_2$)

	$d_{(101)}$(Å)	$d_{(200)}$(Å)	a(Å)	c(Å)
TiO_2	3.52	1.893	3.786	9.502
$Pb_xTi_{1-x}O_2$	3.52	1.899	3.798	9.373

has also been observed for the Pb doped TiO_2 film. However, the d value (3.01 Å) obtained is slightly less than that given in the JCPDS powder diffraction card (3.1 Å) for (101) plane of α–PbO [12], which may be due to presence of Ti [4].

5.3.4 *Scanning electron microscopy*

The scanning electron micrograph of 10 mol % Pb doped TiO_2 thin film, shown in Fig. 5.6(a), reveals nano–crystalline nano–porous structure of the film with high surface area where the particles are interconnected in a three dimensional network. Clear spherical particles, with average particle size ranging from 10 to 15 nm, along with particles of much smaller size, can be observed from this micrograph. The presence of smaller particles may be due to the presence of PbO in nanocrystalline form as also observed by the XRD pattern (Fig. 5.5, pattern b). The cross-sectional view of the same film is shown in Fig. 5.6(b) which shows that the pores are present not only at the surface, but are distributed along the thickness of the film.

5.3.4 *X–ray photoelectron spectroscopy*

XPS analyses were carried out to determine the composition of the film and identify the valence states of various species present therein. Figure 5.7 shows the XPS depth profiling of 10 mol % Pb doped TiO_2 thin film. No trace of any impurity has been observed in the film except carbon, which is found only in a few top layers of the film. As can be seen from Fig. 5.7, Pb, Ti and O are distributed almost uniformly in the film. However, at the surface Pb concentration is much higher than that in the interior of the film. This point is illustrated in Fig. 5.8 where the atomic ratio Pb/Ti is plotted against the sputtering time along the thickness of the film. The value of Pb/Ti at the surface, which is 0.267, is much higher than the actual doping concentration which is only 10 mol %, i.e., a value of 0.1 for Pb/Ti, and clearly shows the enrichment of Pb near the surface as has also been observed by others for sol-gel derived Pb-contained films [13-16]. Below the surface, Pb concentration decreases rapidly and in the interior of the film Pb/Ti ratio reaches a value of around 0.063. This

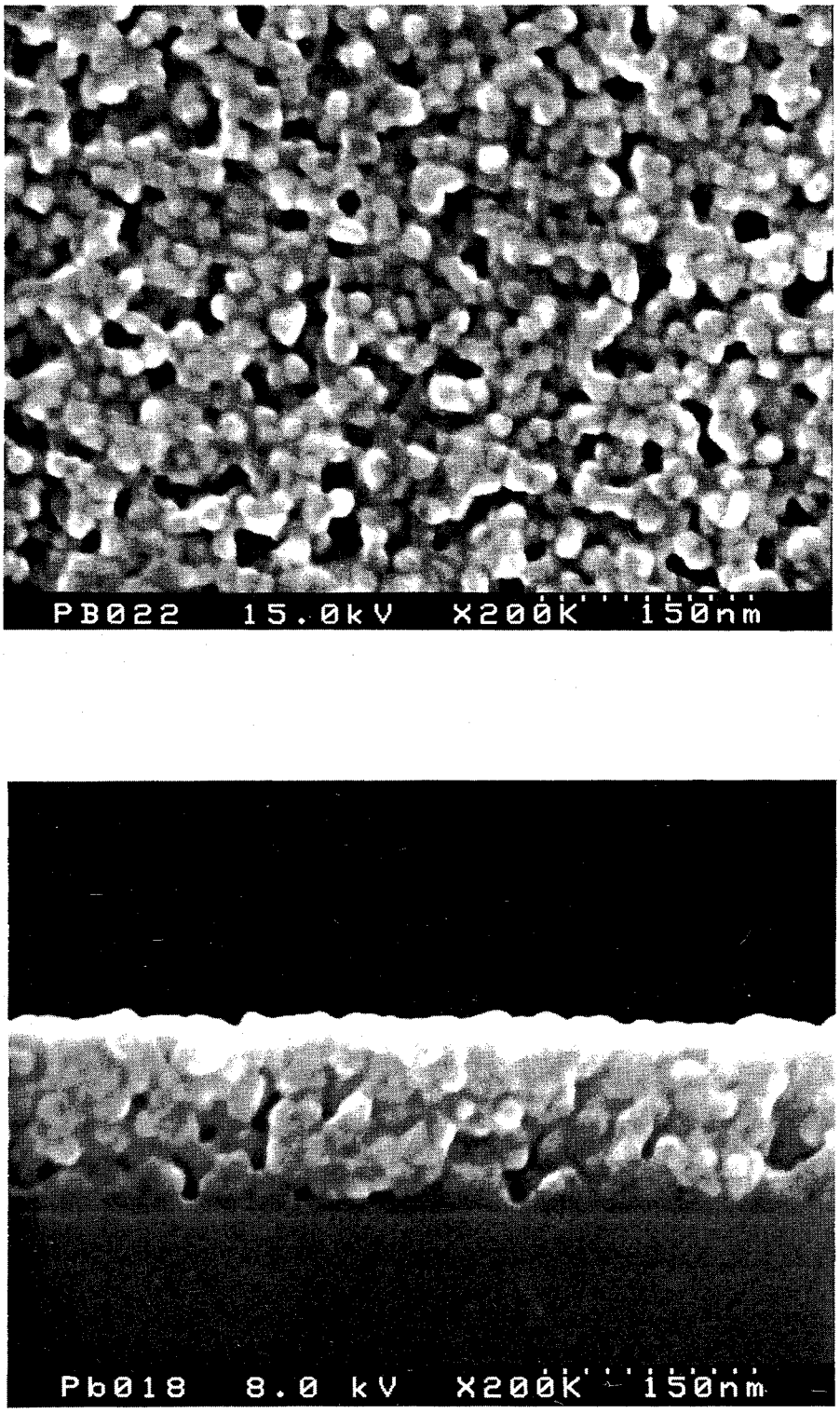

Fig. 5.6 SEM surface morphology (top) and cross-sectional view (bottom) of 10 mol % Pb doped TiO_2 thin film deposited on Si substrate.

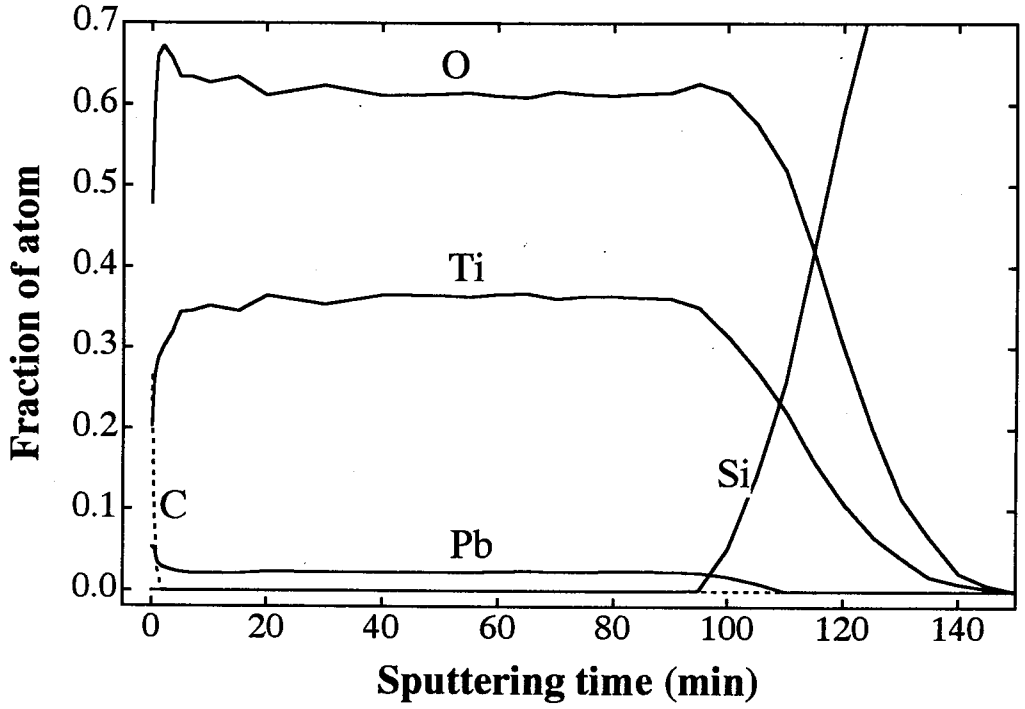

Fig. 5.7 XPS depth profiling of 10 mol % Pb doped TiO_2 thin film deposited on Si substrate, shows uniform distribution of Pb, Ti and O along the thickness of the film.

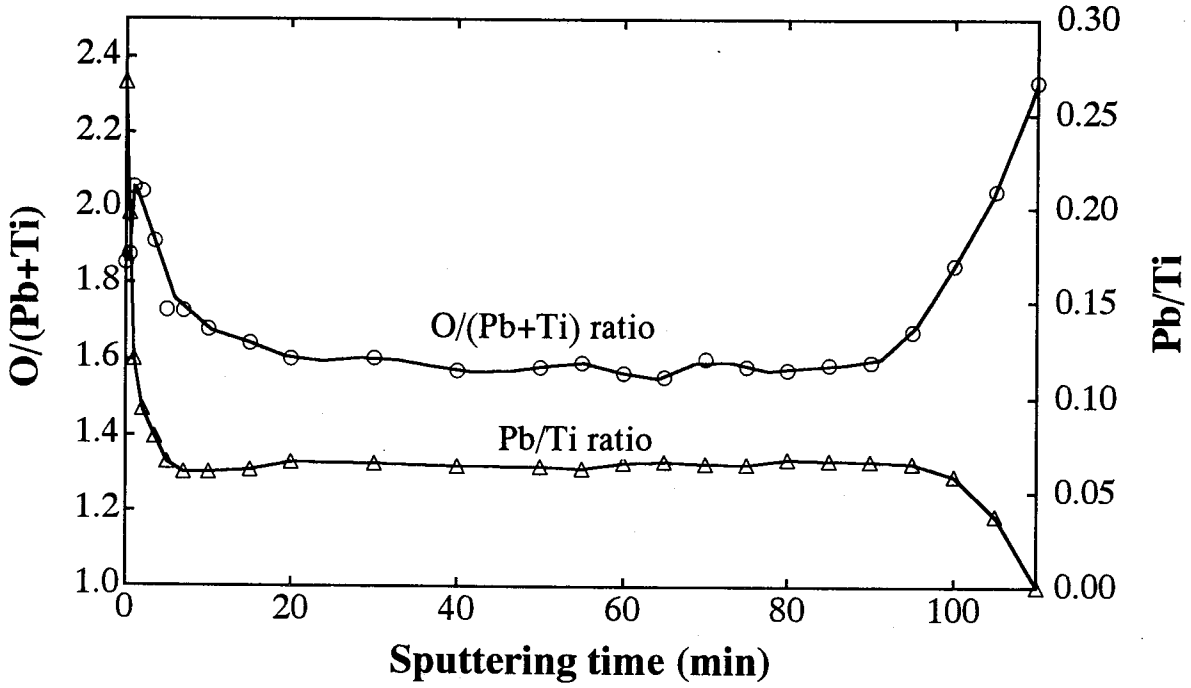

Fig. 5.8 Pb/Ti and O/(Pb+Ti) atomic ratios, along the thickness, plotted against the sputtering time for 10 mol % Pb doped TiO_2 thin film deposited on Si substrate.

This decrease in Pb/Ti to below 0.1 may be understood from the fact that Ar^+ ion bombardment causes faster removal of Pb than Ti and thereby a decrease in the value of Pb/Ti than the actual value in the interior of the film [17]. Except for the Pb enrichment near the surface, which is a common

phenomenon for sol-gel derived Pb-contained films, our film shows almost uniform distribution of Pb along the thickness of the film. This was further confirmed by EDAX analysis carried out over the cross-section of the film at different depths from the surface, which revealed homogeneous distribution of Pb and Ti.

Besides the Pb/Ti plot, a plot of O/(Pb + Ti) ratio is also shown in Fig. 5.8. At the surface, though the ratio is close to 2, it decreases rapidly below the surface and reaches around 1.6 in the interior of the film. The decrease in O/(Pb + Ti) ratio at the beginning may be due to the preferred sputtering of O with respect to Ti, after which a dynamic equilibrium is reached and the O/(Pb + Ti) ratio reaches a near constant value in the interior of the film [18].

The XPS spectra of Pb 4*f*, Ti 2*p* and O 1*s* peaks of the film before and after Ar^+ ion bombardment are shown in Figs. 5.9, 5.10 and 5.11, respectively. As it can be seen from Fig. 5.9, there is a large decrease in the peak intensities in spectra (b) and (c), which are taken after 3.5 and 10 min of Ar^+ ion bombardment, respectively, compared to those of spectrum (a) taken at the surface. The relatively large intensity of the peaks at the surface indicates Pb segregation which has already been discussed above. Spectrum (c), which is deconvoluted using 100% gaussian fitting, shows the presence of both Pb^{4+} and Pb^{2+} states. A reasonably good fit has been obtained between the measured (dotted line) and fitted (solid line) spectra. The binding energies and the full widths at half maximum (FWHM) of Pb 4*f* transitions corresponding to two oxidation states, obtained from the deconvoluted spectra, are listed in Table 5.2 and are in reasonable agreement with those reported in the literature [19, 20].

The origin of the tetravalent lead could be due to the incorporation of lead as a tetravalent ion in the TiO_2 lattice and hence the phase $Pb_xTi_{1-x}O_2$. The presence of Pb^{2+} state indicates the presence of excess lead, presumably in the form of lead oxide (PbO) as has already been revealed by the XRD results. Also, as it can be seen from Fig. 5.9, the peak intensity corresponding to Pb^{2+} state increases significantly from spectrum (c) to (b) and from spectrum (b) to (a), where it is much stronger than the Pb^{4+} peak intensity, indicating that most of the excess lead near the surface, which is

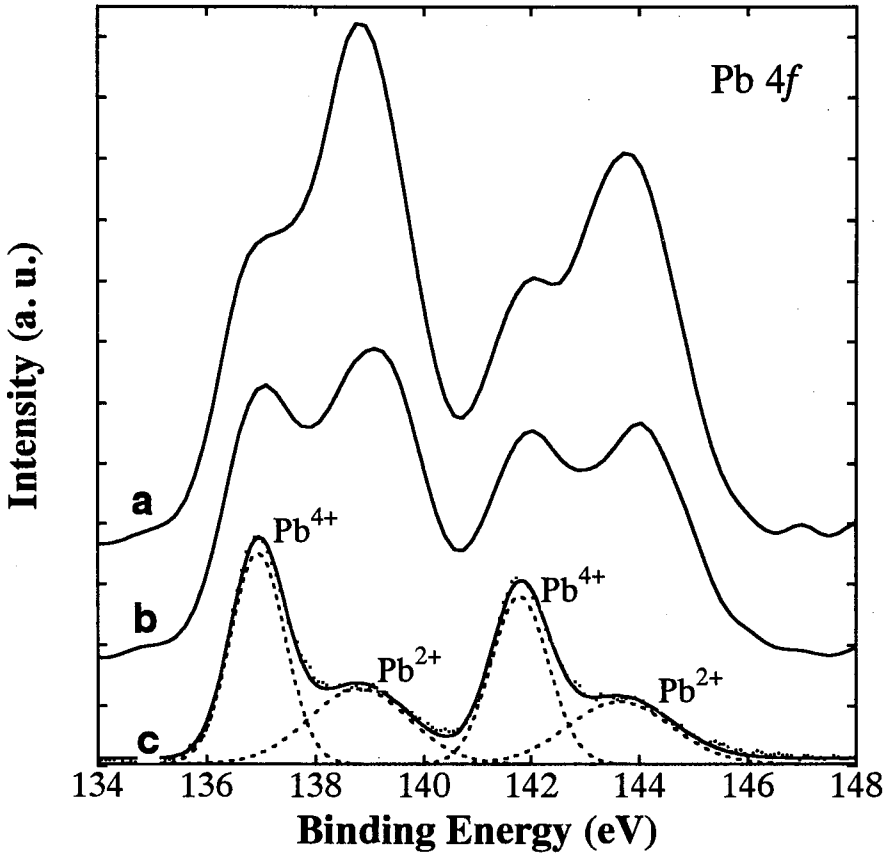

Fig. 5.9 XPS spectra of Pb 4*f* peaks of the 10 mol % Pb doped TiO_2 thin film taken before (a), and after 3.5 (b) and 10 (c) minutes of Ar^+ ion bombardment. The dotted and the solid lines in spectrum (c) are the measured and fitted data respectively. The dashed lines show the deconvoluted spectrum for (c).

Table 5.2 Ti (2*p*) and Pb (4*f*) XPS data obtained from the deconvoluted spectra taken after 10 min of Ar^+ sputtering

Oxidation state	Binding energy (eV)		FWHM (eV)
	$(2p_{3/2})$	$(2p_{1/2})$	$(2p_{3/2})$
Ti (IV)	459.3	464.61	2.5
Ti (III)	457.27	462.34	2.11
Ti (II)	455.55	461.41	1.95
	$(4f_{7/2})$	$(4f_{5/2})$	$(4f_{7/2})$
Pb (IV)	136.95	141.8	1.25
Pb (II)	138.83	143.67	2.0

due to the surface segregation, is in divalent state in the form of PbO. However, there is a possibility that Ar^+ ion etching may cause reduction of PbO to elemental Pb and, thereby, decrease the XPS peak intensity corresponding to Pb^{2+} state. Wang *et al.* reported the presence of both Pb and PbO in $PbTiO_3$ when it was bombarded by 200 keV Ar^+ ion [21]. Unlike the high acceleration voltage used by Wang *et al.* where their main objective was ion implantation, a much smaller acceleration voltage (3 keV) has been used in our experiment which is less likely to reduce PbO to elemental Pb. However, in order to verify the results, XPS spectra of Pb 4*f* peak of pure PbO are recorded both at the surface and at depths under the same etching conditions as has been used in our experiment, i.e., an acceleration voltage of 3 keV and a beam current of 3 mA, and less than 5% of PbO has been observed to get reduced to Pb even after 30 minutes of Ar^+ ion etching. This result clearly shows that while the Pb^{2+} state may get reduced to Pb to some extent by Ar^+ ion bombardment, the large decrease in Pb^{2+} peak intensity with etching time can not be attributed to Pb^{2+} reduction and is most probably due to surface enrichment. In contrast to the large change in the Pb^{2+} peak intensity, the change in Pb^{4+} peak intensity is much less, and the small decrease from spectrum (a) to (b) and from (b) to (c) may be due to the preferred sputtering and surface enrichment of Pb, which in another way indicates almost uniform distribution of Pb^{4+} state, and hence the material $Pb_xTi_{1-x}O_2$, along the thickness of the film.

The XPS spectra of the Ti 2*p* peak are shown in Fig. 5.10 and also show a doublet structure like Pb 4*f* peak. Before Ar^+ ion bombardment, the Ti $2p_{3/2}$ peak is narrow with slight assymmetry and has a binding energy of around 459 eV, a value little larger than that of Ti^{4+} state in TiO_2 (458.3 eV), which may be due to the incorporation of Pb into TiO_2. The Ti 2*p* spectrum, taken after 3.5 and 10 minutes of Ar^+ ion bombardment (spectra (b) and (c)) are broad and more assymetric. Spectrum (c) is deconvoluted and it shows the presence of three doublets with peak energies matching with divalent, trivalent and tetravalent states of Ti. The binding energies and FWHM of Ti 2*p* transitions corresponding to various valence states obtained from the deconvoluted spectra are tabulated in Table 5.2 and are in good agreement with those in the literature [4,16,17]. A close inspection of the three spectra, (a), (b) and (c) in Fig. 5.10, reveals that spectrum (a) consists mostly of Ti^{4+} state with a small

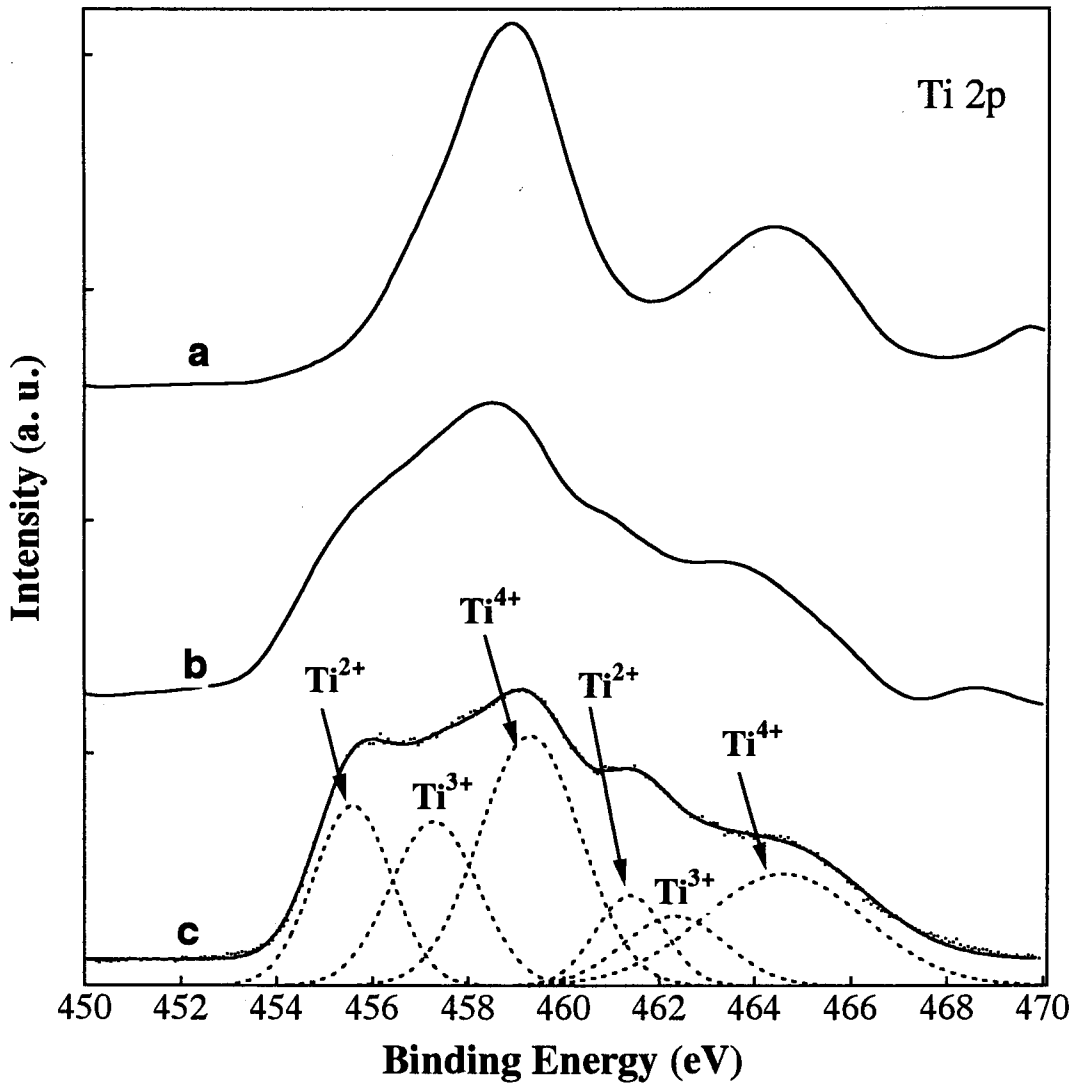

Fig. 5.10 XPS spectra of Ti 2*p* peaks of the 10 mol % Pb doped TiO_2 thin film taken before (a), and after 3.5 (b) and 10 (c) minutes of Ar^+ ion bombardment. The dotted and the solid lines in spectrum (c) are the measured and fitted data respectively. The dashed lines show the deconvoluted spectrum for (c).

content of Ti^{3+} state; spectrum (b) consists of both Ti^{3+} and Ti^{2+} states along with Ti^{4+} state, and spectrum (c) also consists of both Ti^{3+} and Ti^{2+} states besides Ti^{4+} state, but in a much increased amount compared to those of spectrum (b). The large increase in Ti^{2+} and Ti^{3+} states in spectra (b) and (c) is attributed to the Ar^+ ion bombardment effect which is known to reduce the transition metals to lower valence states [18]. This gradual reduction of TiO_2 due to Ar^+ ion bombardment is also reflected in the O 1*s* spactra, taken at the surface and after 3.5 and 10 minutes of sputtering, which are shown in Fig. 5.11. A certain assymetry, broadening on the high binding-energy side, is evident in all the

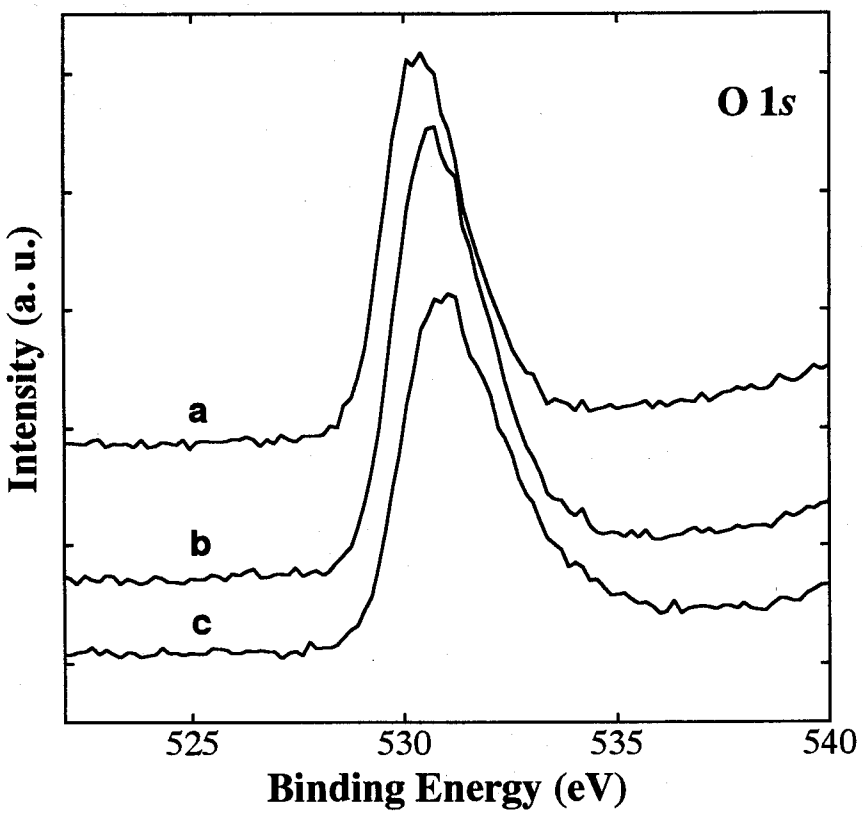

Fig. 5.11 XPS spectra of O 1*s* peaks of 10 mol % Pb doped TiO_2 film deposited on Si substrate taken before (a), and after 3.5 (b) and 10 min (c) of Ar^+ ion bombardment.

spectra and increases with increased Ar^+ ion bombardment with a simultaneous shift of the peak towards higher energy. The O 1*s* spectrum of pure TiO_2 is sharp and symmetric with a binding energy of around 530 eV and an assymetry in the spectrum, resulting from the overlapping of multiple spectra, shows the reduced characteristics of TiO_2 [22–24]. The slight assymetry of the O 1*s* spectrum taken at the surface may be related with the presence of Ti^{3+} as well as PbO in the film as has already been confirmed from the Ti 2*p* and Pb 4*f* spectra, and the increased assymetry in the interior of the film can be related with increased reduction of TiO_2 with Ar^+ ion bombardment.

5.4 Conclusions

Pure, and 5 and 10 mol % Pb doped TiO_2 thin films have been prepared by a sol–gel dip–coating method for a future novel low–cost solid–state solar cell application. Optical gap energies estimated from the transmission measurements for pure, and 5 and 10 mol % Pb doped TiO_2 are 3.14,

3.05 and 2.74 eV, respectively, which show a decrease of 0.25 and 0.5 eV in the optical gap energy for 5 and 10 mol % Pb doped TiO_2, respectively, from that of pure TiO_2. PL measurement also shows a gradual shift of the emission peak towards longer wavelength, i.e., lower energy region, and supports the lowering of the optical gap of TiO_2 upon Pb doping.

XRD results of both pure and Pb doped TiO_2 reveal that the films are polycrystalline with crystal structure matching with anatase modification of TiO_2. Films are found to be oriented predominantly in A(101) plane with slight shift in the d spacing for the Pb doped film confirming the incorporation of Pb into TiO_2 lattice. Elemental analysis by XPS reveals that except for the Pb enrichment near the surface, Pb, Ti and O are distributed uniformly along the thickness of the film. Further, Pb has been found in both divalent and tetravalent states with the divalent state predominating near the surface of the film. Presence of Pb^{2+} indicates that there remains excess lead in the film which could not be incorporated into TiO_2 and most probably it is in PbO form as has also been observed by XRD. This argument is further substantiated by the fact that Pb^{2+} state is highly concentrated near the surface where Pb enrichment has occurred. Presence of Pb^{4+} state could be due to the incorporation of Pb into TiO_2 lattice as a tetravalent ion and confirms the formation of $Pb_xTi_{1-x}O_2$.

However, further incorporation of Pb into TiO_2 is needed to reduce the energy gap more, which should be around 2.58 eV, and thereby increase the electron affinity so as to match the conduction band position of $Pb_xTi_{1-x}O_2$ with that of $CuInSe_2$ in order to obtain the theoretically predicted efficiency of 18% [2]. Further efforts, therefore, are necessary to prepare single phase $Pb_xTi_{1-x}O_2$ film with desired electro-optical characteristics for the fabrication of a low-cost solid-state heterojunction n-$Pb_xTi_{1-x}O_2$/p-$CuInSe_2$ solar cell.

References

[1] B. O' Regan and M. Gratzel, *Nature* **353** (1991) 737.

[2] M. M. Rahman, T. Soga, T. Jimbo and M. Umeno, *Jpn. J. Appl. Phys.* **35** (1996) 3334.

[3] K. M.Krishna, M. Sharon, M. K. Mishra and V. R. Marathe, *Chem. Phys.* **163** (1992) 401.

[4] K. M. Krishna, M. Sharon, M. K. Mishra, *J. Phys. Chem. Solids* **57** (1996) 615.

[5] K. M. Krishna, M. Sharon, M. K. Mishra, *J. Mater. Sci. Let.* **15** (1996) 1084.

[6] M. M. Rahman, T. Miki, K. M. Krishna, T. Soga, K. Igarashi, S. Tanemura and M. Umeno, *Mater. Sci. Engg. B* **41** (1996) 67.

[7] H. Tang, K. Prasad, R.Sanjines, P.E. Schmid, and F.Levy, *J. Appl. Phys.* **75** (1994) 2042.

[8] H. Tang, H. Berger, P. E. Schmid, and F. Levy and G. Burri, *Solid State Commun.* **87**, (1993) 847.

[9] S. J. Milne and S. H. Pyke, *J. Am. Ceram. Soc.* **74** (1991) 1407.

[10] N. J. Phillips, M. L. Calzada and S. J. Milne, *J. Non-Cryst. Solids* **147** (1992) 285.

[11] U. Selvaraj, A. Prasadaro and S. Komarneni, *Mat. Letts.* **20** (1994) 71.

[12] JCPDS Powder Diffraction File Cards (1994), 21–1272 (TiO_2–anatase), 5–561 (α–PbO).

[13] S. Ibuki, T. Nakayama, M. Okuyama and Y. Hanakawa, *Jpn. J. Appl. Phys.* **29** (1990) 532.

[14] S. S. Dana, K. F. Etzold and J. Clabes, *J. Appl. Phys.* **69** (1991) 4398.

[15] Z. H. Qian, D. Q. Xiao, J. G Zhu and Z. S. Li, *J. Appl. Phys.* **74** (1993) 224.

[16] M. J. Bozack, J. R. Williams, J. M. Ferraro, Z. C. Feng and Jr. R. E. Jones, *J. Electrochem. Soc.* **14** (1995) 485.

[17] C. J. Lu, A. X. Kuang and G. Y. Huang, *J. Appl. Phys.* **80** (1996) 202.

[18] S. Hofmann, in *Practical Surface Analysis*, D. Briggs and M.P. Seah (eds), John Wiley, New York, 1983, p. 161.

[19] J. M. Thomas and M. J. Tricker, *J. Chem. Soc., Faraday Trans. II* **71** (1975) 329.

[20] K. S. Kim, T. J. O'Leary and N. Winograd, *Ananl. Chem.* **45** (1973) 2214 and

references therein.

[21] Y. G. Wang, B. D. Qu, W. L. Zhong, P. L. Zhang, and K. M. Wang, *J. Appl. Phys.* **72** (1992) 3726.

[22] C. N. Sayers and N. R. Armstrong, *Surf. Sci.* **77** (1978) 301.

[23] D. Robba, D.M. Ori, P. Sangalli, G. Chiarello, L. E. Depero and F. Parmigiani, *Surf. Sci.* **380** (1997) 311.

[24] A. Azoulay, N. Shamir, E. Fromm and M. H. Mintz, *Surf. Sci.* **370** (1997) 1.

Chapter 6

Summary

There is a long standing need for cheap and clean energy sources as the world population continues to increase with an increasing energy consumption per person. Use of fossil fuels and nuclear plants in an increasing rate to meet the energy demand poses a serious threat to environment as well as to their availability. A frequently mentioned solution to the problem of increasing requirements for energy and dwindling energy sources is to tap the energy in sunlight. The solar energy falling on the earth's surface each year is over 20,000 times the amount presently required by the human race, making for a seemingly inexhaustible supply. Until now, solar cells are regarded as the prime candidate for solar energy conversion for effective utilization by human civilization. However, the various solar cells fabricated to date are far too expensive to use on a commercial basis. This dissertation is aimed at developing a low cost solar cell based on low cost semiconducting material TiO_2 for common consumer application.

Chapter 1 is devoted to a brief discussion about the importance of solar cells as a clean and inexhaustible energy source and evolution of TiO_2 as a potential candidate for cheap solar cell material. A breakthrough work by Gratzel and his group in preparing a low-cost efficient photoelectrochemical (PEC) cell, based on dye sensitized nano-crystalline (DNC) TiO_2 of anatase type, has opened the prospect of cheap and renewable energy for common consumer use. However the dye solar cell, which is yet to commercialize, suffers a lack of stability due to liquid electrolyte and the dye. These drawbacks are outlined in chapter 1 and a solid state prototype of the DNC cell based on TiO_2 is proposed. The purpose and organization of this dissertation are also outlined.

TiO_2 exists in three crystal modifications: rutile, anatase and brookite, among which rutile is known to be the most stable phase and its properties are well studied. After Gratzel's dye solar cell, anatase modification of TiO_2 came into focus because of its high photon to current conversion efficiency which is nearly 100%. Therefore, it is worth investigating the properties of TiO_2 thin films, specially that of anatase type. In chapter 2, we have presented a detailed structural, optical and electrical analyses of our sol-gel derived TiO_2 thin films, deposited on different substrates under different annealing temperatures, using standard techniques with the main attention focused on the anatase modification of TiO_2. Films deposited under same condition on different substrates showed different structural properties. The as-deposited films on sapphire and silicon substrates were polycrystalline, anatase type, while that on the quartz substrate was amorphous in nature. Up to 600 °C annealing temperature, films were polycrystalline, single phase, anatase type for all the substrates, above which (800 °C) films were rutile (on quartz and sapphire substrates) or a mixture of A/R (on Si substrate), depending upon substrate topography. Optical gap energies estimated from UV-visible transmittance and reflectance measurement are 3.25 and 3.15 eV for amorphous and anatase TiO_2, respectively. Conductivity study shows the nano-crystalline films to be highly resistive, in the range of 10^6~10^9 Ω-cm, with the conductivity across the film almost 3 order of magnitude higher than that along the surface of the film. Pure anatase films revealed good photoconductivity, of the order of 3 −4, and both the dark and photoconductivity increased upon annealing in H_2 atmosphere up to 700 °C annealing temperature.

In chapter 3, the new type of PEC solar cell developed by Gratzel and his group, namely, dye-sensitized nano-crystalline TiO_2 solar cell, is introduced and some results of our preliminary investigation on this cell fabricated in our lab are presented. A brief historical review of this cell is also given to help understand some of the basic features of the cell. The cell can be prepared from medium purity materials using low-cost process. Further, the materials used are environmentally benign removing any concern of environmental pollution.

The TiO_2 thin films, used to prepare DNC cells, were deposited by (i) spreading of TiO_2

colloidal sol using a glass rod and (ii) sol-gel dip-coating method. In the glass rod spreading method, effect of triton-X addition to the colloidal sol of TiO_2 on the film surface morphology and cell performance has been studied. Slight amount of triton-X addition to the sol has been found to have a profound effect on the surface morphology and cell performance. Almost five times increase in the short-circuit current has been observed for the cell with triton-X than that of the cell without triton-X. Densely populated large cracks are observed for the TiO_2 films that were prepared using the sol which contains no triton-X. Slight addition (0.25 vol %) of triton-X assist in spreading the sol on the substrate and, thereby, the formation of a smooth surface. However, excess amount of triton-X addition results in reformation of the cracks and degradation of the cell performance. Highest efficiency and fill factor has been obtained for the cell with 0.5 vol % of triton-X addition. It is concluded that the best performance of a cell can be obtained with maximum amount of triton-X addition for which no crack formation takes place.

In the sol-gel dip-coating method, the effect of pulling speed on the cell performane has been studied. For the cell with pulling speed of 0.1 mm/s, the cell efficiency was quite low,only 0.3%, though the film thickness was around 400 nm. With the increase in the pulling speed, as the film thickness increased, the cell efficiency also increased and rose over 1% at a pulling speed of 0.5 mm/s. One major advantage of this method is this that very thin (few tens of nm to several 100 nm) and highly transparent films of TiO_2 on large substrate can be deposited by this method which can be used to develop transparent or semi-transparent DNC cells suitable for window application. Transmittance of a typical DNC cell prepared using sol-gel derived TiO_2 films showed high transparency, with the highest 65% at 650 nm and near or over 50% almost in the whole visible region which demonstrates its suitability for window application.

Though the DNC cell is very attractive because of its low-cost and simple fabrication process, it has some practical problem like stability which has already been mentioned. Therefore, it is important to develope a solid-state cell which will be stable while at the same time cheap and efficient. In chapter 4, a solid-state solar cell based on the low-cost material TiO_2 (n–TiO_2/p–$CuInSe_2$) has been

proposed and a model for calculating the efficiency of the cell is developed. However, because of the high barrier height ($\Delta E_C = 0.48$ eV) at the junction, efficiency was found to be quite low (1.51%) under ideal conditions, i.e., neglecting recombination losses and assuming zero series and shunt resistances. To reduce the high barrier at the junction, a new solar cell material $Pb_xTi_{1-x}O_2$, where both the band gap and electron affinity can be varied by varying x, is proposed as the top material of the cell instead of TiO_2 and a model is also developed to calculate the cell efficiency. Assuming $\Delta E_C = 0$ for *n*–$Pb_xTi_{1-x}O_2$/*p*–$CuInSe_2$, an efficiency of 18.78% has been obtained at 1 SUN AM 1.5 conditions. The effects of doping concentration and cell thickness on the cell performance are also studied. It is found that the cell performance is little affected by the window layer parameters, due to negligibly small contribution of window region to the total photocurrent which is again due to the very small minority carrier diffusion length and mobility in this region.

Chapter 5 is devoted totally to the preparation and characterization of $Pb_xTi_{1-x}O_2$ film for a solid-state solar cell application as proposed in the theoretical work of chapter 4. Pure, and 5 and 10 mol % Pb doped TiO_2 thin films have been prepared by a simple sol-gel dip-coating method. Optical gap energies estimated from the transmission measurements for pure, and 5 and 10 mol % Pb doped TiO_2 are 3.2, 2.95 and 2.7 eV, respectively, which show a decrease of 0.25 and 0.5 eV in the optical gap energy for 5 and 10 mol % Pb doped TiO_2, respectively, from that of pure TiO_2. PL measurement also shows a gradual shift of the emission peak towards longer wavelength, i.e., lower energy region, and supports the lowering of the energy gap of TiO_2 upon Pb doping.

XRD results of both pure and Pb doped TiO_2 reveal that the films are polycrystalline with crystal structure matching with anatase modification of TiO_2. Films are found to be oriented predominantly in A(101) plane with slight shift in the d spacing for the Pb doped film confirming the incorporation of Pb into TiO_2 lattice. Elemental analysis by XPS reveals that except for the Pb enrichment near the surface, Pb, Ti and O are distributed uniformly along the thickness of the film. Further, Pb has been found in both divalent and tetravalent states with the divalent state predominating near the surface of the film. Presence of Pb^{2+} indicates that there remains excess lead in the film which

could not be incorporated into TiO_2 and most probably it is in PbO form as has also been observed by XRD. Presence of Pb^{4+} state could be due to the incorporation of Pb into TiO_2 lattice as a tetravalent ion and confirms the formation of $Pb_xTi_{1-x}O_2$.

In conclusion, prospect of photovoltaic solar cells based on the low-cost material TiO_2, both liquid junction and solid-state type, is explored. The dye solar cell with its low-cost and simple proceesing technique is very attractive. The DNC cell can be made semi-transparent to transparent depending upon the thickness of the TiO_2 film which is suitable specially for power window application. However, much remains to understand fully the device operation mechanism and effects of various parameters, such as particle size, porosity, defect density, film thickness, electrolyte concentration, etc., on the cell performance, and a detailed study is necessary to improve the present status of the cell.

In order to overcome the lack of stability of the DNC cell, a solid-state heterojunction solar cell has been proposed where effcicieny as high as 18 % can be obtained according to the theoretical calculations. Results on our preliminary attempt to prepare $Pb_xTi_{1-x}O_2$ film reveal the possibility of decreasing the band gap and thereby changing the electron affinity of TiO_2 by doping it with Pb. However, Further efforts are necessary to prepare single phase $Pb_xTi_{1-x}O_2$ film with desired electro-optical characteristics for the fabrication of a low-cost solid-state heterojunction $n-Pb_xTi_{1-x}O_2/p-CuInSe_2$ solar cell. Preparation of single phase $Pb_xTi_{1-x}O_2$ film with a desired value of x, such that the conduction band edge of $Pb_xTi_{1-x}O_2$ matches perfectly with that of $CuInSe_2$ so as to produce the theoretically predicted heterojunction solar cell, will be the future scope of this work. Special care is needed to get a high quality, single phase $Pb_xTi_{1-x}O_2$ film. This can be achieved by modifying the current sol-gel process or employing any other suitable method such as ion implantation or gas phase techniques. Apart from the solar cell aspect, the material $Pb_xTi_{1-x}O_2$ also shows a promise for photocatalytic applications. Since it has a lower optical gap and can harness greater part of the solar energy, higher yield can be expected from this material than that of TiO_2.